International Science Journal
(Peer-Reviewed)
ISSN: 2348 – 604X (p); 2348 – 6058 (e)
DAMA INTERNATIONAL

STUDIES ON THE OPTICAL PROPERTIES OF MN DOPED ZNS NANOPARTICLES

[1]Shashank Sharma, Ravi Sharma
[1]Mechanical branch, 6th sem BIT Durg (C. G.), INDIA
Department of Physics, Govt. Arts and Commerce Girls College Raipur, (C.G.), 492001, INDIA
***email: rvsharma65@gmail.com**

ABSTRACT
The present paper reports the synthesis and characterization of luminescent nanocrystals of zinc sulphide doped with manganese. Nanocrystals of zinc sulphide were prepared by chemical precipitation method using the solution of zinc chloride, sodium sulphide, manganese chloride and mercaptoethanol (ME), used as the capping agent. The particle size of nanocrystals was calculated both theoretically and experimentally. The particle sizes measured by the theoretical model (EMA) and experimentally by XRD, TEM pattern was found to be in the range 1nm-4nm. SEM images showed the agglomeration of nanocrystals. The blue-shift in absorption spectra was observed with reducing size of the nanoparticles. The FTIR spectra inferred that the stabilizing agent passivated the surface of the particles. The blue-shift in the peak position of photoluminescence (PL) spectra was also observed for the samples with decreasing particle size. The maximum PL intensity was recorded for the sample with 1.2 % of Mn.

KEYWORDS: **Nanoparticles; Structural properties; photoluminescence; optical absorption spectra; ZnS:Mn.**

1. INTRODUCTION

Materials in the nanometer scale may exhibit physical properties, distinctively different from that of bulk [Cao G. (2014)]. Decrease in the particle size gives rise to quantum confinement effect, wherein an increase in the energy gap as well as splitting of the conduction and valence band into discrete energy levels becomes evident. These particles have promising potential applications in nonlinear optics, light emitting materials and optoelectronics.

The II-VI semiconductor ZnS is used in many applications primarily for its luminescent properties. The luminescence of ZnS has been studied by many workers [Karar N., Singh F., Mehta B.R., J. (2004), Nanda J., Sarma D.D., (2001), Bol A.A., and Meijerink A., (2001), Bhargava R.N., et. al (1994), Que W., et al (1998), Borse P.H. et. al.(1999) Strukov D.B., et al (2008)]. ZnS is a commercially important II–VI semiconductor having a wide optical band gap, rendering it a very attractive material for optical application especially in nanocrystalline form. ZnS can have two different crystal structures (zinc blende and wurtzite). It is a direct band gap material having band gap energy 3.67eV and a small exciton Bohr radius of ~ 4 nm. Owing to its wide band gap, it is used in cathode ray tube, the field emission display, and the scintillator as one of the most frequently used phosphors [Okuda H., et al (1990), Ghrayeb J. et al (1997) Barton J.C., Ranby P.W., (1997)]. In addition, a ZnS crystal laser has been produced using streamer excitation, and thin films of ZnS can be used as an active emitting material in such a device, termed the hot electron cold cathode [Dalacu N., Kitai A.H. (1991)]. Optical and luminescent properties of nanocrystalline ZnS prepared in the forms of thin film, powder and colloide using different synthesis techniques such as sputtering [Mandal S.K., Chaudhuri S., Pal A.K. (1999)], co-evaporation [Thielsch R., Böhme T., Böttcher H. (1996)], wet chemical [Chen W., et al (1997), Scholtz S.M., et al (1998), Nanda J., et al (2000)], sol-gel [Tan M., Cai W., Zhang L.(1997), Bhattacharjee B. et al (2003)] solid state [Lu H.-Y. et al (2004)], micro-wave irradiation [Zhao Y., Hong J.-M., Zhu J. (2004), Ni Y., Yin G., Hong J. Xu, Z. (2004)], ultrasonic irradiation [Xu J.F. et al (1998)] or synthesis under high-gravity environment [Chen J. et al (2004)] were studied in detail.

In the present work, we report the chemical route synthesis of ZnS:Mn nanoparticles and their characterization by XRD, SEM,TEM, UV-VIS spectrometry and PL spectrometry. The effect of concentration of the capping agent on the particle size, structural, morphological and optical properties of the nanocrystals was investigated. The study was aimed to optimize the concentration of the capping agent by structural and optical characterization.

2. EXPERIMENTAL

Chemical route is used in the present investigation. All the reagents were of AR-grade and used without further purification. The powder of ZnS nanoparticles were prepared by using chemical deposition technique described by Khosravi [Khosravi A.A. et al (1995)]. In this method aqueous solution of zinc chloride ($ZnCl_2$), mercaptoethanol (C_2H_5OSH) and sodium sulphide (Na_2S), each of 1M was prepared and equal volume of each solution was used for the reaction. Firstly, the $ZnCl_2$ solution was taken in a reaction vessel and mercaptoethanol was added to it drop wise, while stirring it continuously. Then sodium sulphide was added dropwise to the same reaction vessel. Solutions were mixed at rate of 1 ml per minute. For doping the ZnS clusters with Mn, $MnCl_2$ was simply added to $ZnCl_2$ solution. The end product was washed thoroughly in double distilled water to remove any excess sodium sulphide which may be present. Finally, the solution was centrifuged at 3500 rpm and the precipitate obtained was air dried. By properly adjusting the concentration of the starting reagents free standing powder of ZnS : Mn nanoparticles were achieved. The prepared ZnS. Mn. nanoparticles were characterized by different techniques.

The morphologies and sizes of the ME capped ZnS:Mn were determined by X-ray diffraction studies with Cu Kα radiation (λ = 1.5418 Å). X-ray diffraction patterns were obtained by Rigaku Rotating Anode (H-3R) diffractometer. XRD data were collected over the range 20°–70° at room temperature. For scanning electron microscope (SEM), JSM – 5,600 LV was used. Transmission Electron Microscope Tecnai 20 G2 (FEI make) was used to take the TEM photograph. The particle size was calculated using the Debye-Scherrer formula. Absorption spectra of the samples prepared with various concentrations of ME was recorded with the help of Perkin Elmer Model Lamda 950 UV-VIS spectrophotometer. The FTIR spectra were recorded by the help of FTIR spectrometer (SHIMADZU) in the range of 500 cm^{-1} to 4,000 cm^{-1}. The powders were first dispersed in water and placed in a quartz cuvette. Pure water was used as the reference sample. For PL measurements Perkin Elmer spectroflurophotometer Model LS 45 was used.

3. RESULTS AND DISCUSSIONS

The XRD spectra of bulk ZnS and synthesized ZnS: Mn particles are shown in Figure1. Figure 1 (Y) shows the XRD pattern of bulk crystals of ZnS: Mn and figure (X) shows the XRD patterns of the synthesized samples of ZnS: Mn nanoparticle. There are some important differences between the diffraction patterns of nano and bulk materials. It can be very clearly seen from the figures (X) that the XRD pattern shows broadening in the peaks. Nanomaterials have small particle size and this causes broadening in their diffraction peak. The broadening of the peak is due to a small number of crystal planes. This broadening in turn causes a loss of intensity in the signal of their diffraction patterns. Bulk materials, on the contrary, have sharp, narrow and high-intensity peaks. The sharp peaks of the bulk particles show that it is highly crystalline and the particles are in the micron size. The three diffraction peaks positions corresponds to the lattice planes of (1 1 1), (2 2 0) and (3 1 1) matching the zinc blende (sphalerite) ZnS crystal structure (JCPDS 5-566). Manganese impurities did not contribute to, any additional diffraction peaks and it indicates that the Mn^{2+} ions were well dispersed in the ZnS matrix and their concentration was relatively low [W.Q. Peng et al (2005)]. Fig.1(X) shows the XRD patterns of ZnS:Mn with different concentration of mercaptoethanol (ME). The concentration of ME was changed from 5drop/100ml to 20drop/100ml. More broadening in the diffraction peaks was observed for the samples with higher concentration of the capping agent. For all the samples the size of the particles were calculated from the first peak only. The average crystallite size calculated using the Scherer's formula was found to be in the range 1.5nm - 3nm [Guinier, A (1963)]. The lattice parameter has been computed as 5.32 Å, which is very close to the standard value (5.42 Å).

A typical SEM image of ZnS nanocrystals is shown in Figure 2. It can be seen that some of the particles are highly agglomerated. It was observed that, synthesis of nanoparticles took place in the first few minute of the experiment and later these particles agglomerates and their size becomes larger. SEM image shows clearly that the particles are not spherical. The average particle sizes obtained from SEM images were found to be in the range of 5nm to 10nm. Some of the particles are even less than 5 nm (encircled).

International Science Journal
(Peer-Reviewed)
ISSN: 2348 – 604X (p); 2348 – 6058 (e)

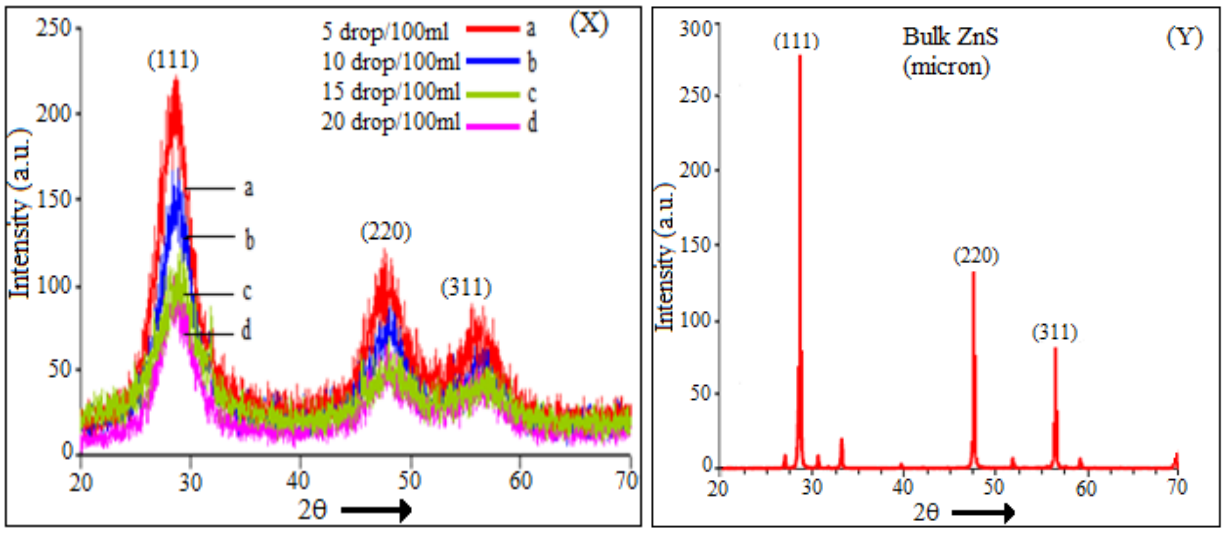

Fig.1 XRD pattern of ZnS:Mn nanocrystals with different concentration of ME

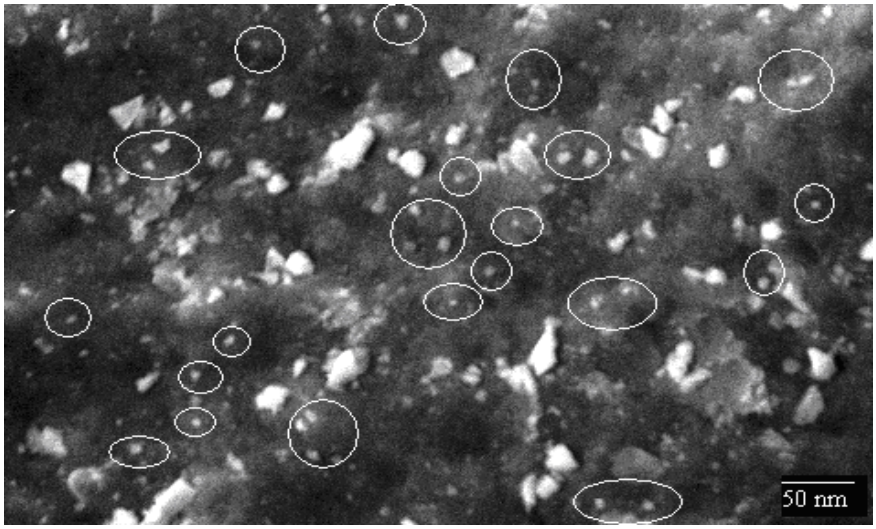

Fig. 2 SEM photograph of ZnS:Mn nanocrystals

International Science Journal
(Peer-Reviewed)
ISSN: 2348 – 604X (p); 2348 – 6058 (e)

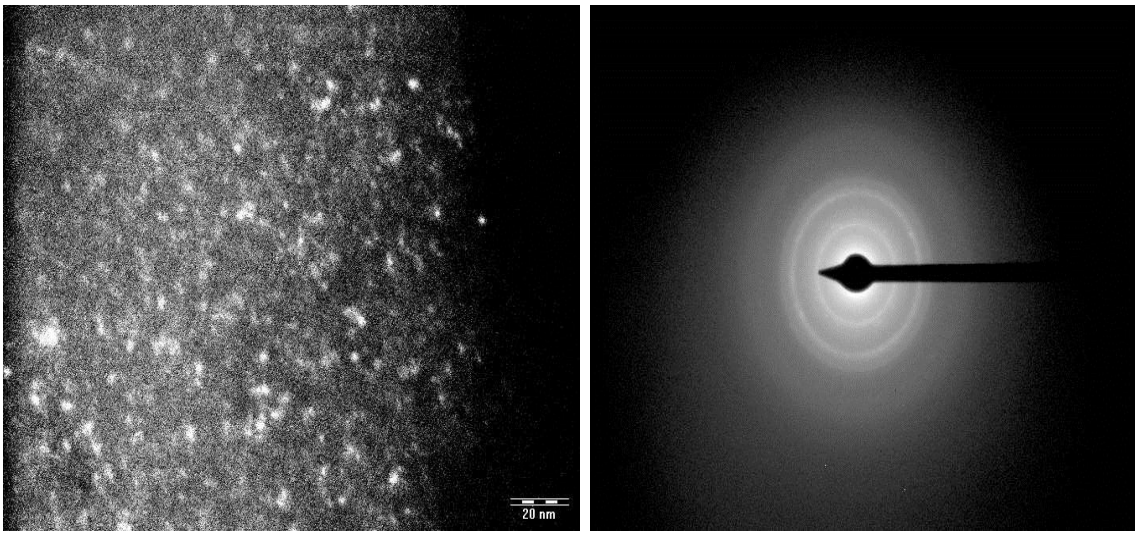

Fig. 3 The Particle size measurement and SAED pattern of ZnS:Mn nanoparticles by TEM

A typical TEM image of ZnS:Mn nanoparticle is shown in Fig.3. The particle sizes obtained from TEM images are found to be in the range of 2nm to 5 nm. Some of the particles are even less than 2 nm. TEM image clearly shows that the particles are not spherical. Few samples were in perfectly in a cubical shape (not shown in the figure). SAED (Selected Area Electron Diffraction) patterns of the samples confirm presence of ZnS cubic structure. The lattice fringes visible in the TEM micrograph are indicative of the crystalline nature of the particles. The three diffraction rings in the ED patterns correspond to the (111), (220), and (311) reflections confirming the cubic zinc blend structure. The three diffraction rings are perfectly indexed to the same positions as those from bulk ZnS.

Figure 4(x) shows the optical absorption spectra of the samples with different molar concentration of the reactants whereas the concentration of capping agent was fixed. The optical absorption spectra were measured between 400 nm-200 nm. It was found that the spectra are featureless and no absorption occurs in the visible region (800 nm-390 nm). Samples with three concentrations of the reactants (10^{-2} M, 10^{-1} M, 1 M) were prepared. It is clear from the figure that the peak of the samples with lower molar concentration (10^{-2} M) shows the shift towards the lesser value of wave length as compared to the higher molar concentration (1 M). The optical absorption edge also showed gradual blue shift for the samples with higher molar concentration of the reactants. The characteristic absorption edge reflects the band gap of the material.

International Science Journal
(Peer-Reviewed)
ISSN: 2348 – 604X (p); 2348 – 6058 (e)

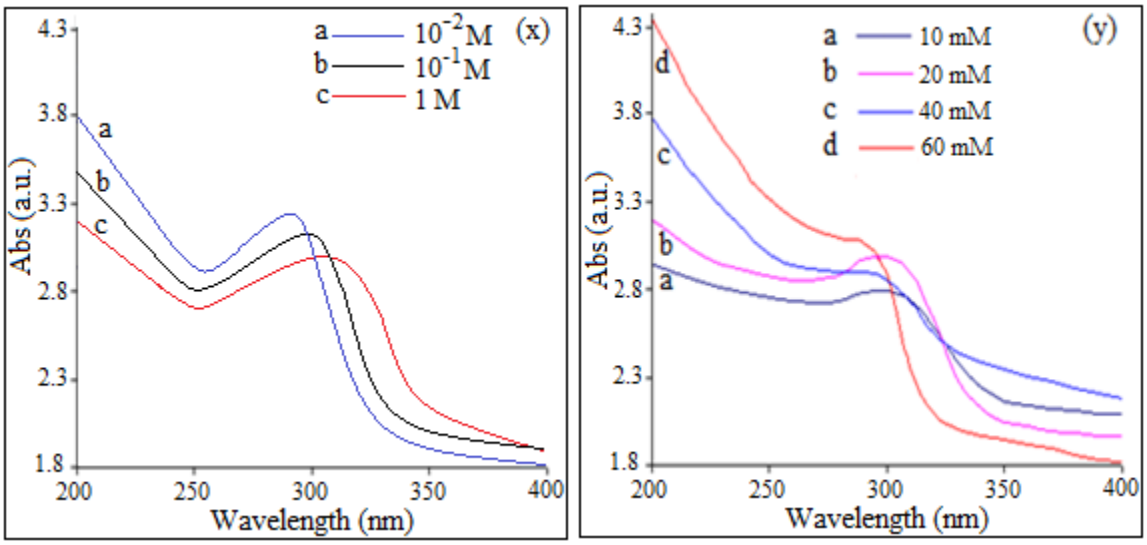

Fig 4(x) Absorption spectra of ZnS:Mn samples with different molar concentration
(y)Absorption spectra of ZnS: Mn nanoparticles with different concentration of ME

Figure 4(y) shows the optical absorption spectra of ZnS: Mn nanoparticles with different concentration of mercaptoethanol (ME). The concentration was changed from 10 mM to 60 mM. The concentration of Mn (1.2 %) was kept constant for all the samples. With the increasing concentration of ME, blue shift in the absorption edge was observed. The observed blue - shift, is the reflection in increase of the band gap owing to quantum confinement effect. The band gap energy of the samples corresponding to the absorption edge was calculated and found between 3.75eV – 5 eV with increasing concentration of the capping agent. Similar results are reported by Kumbhojkar et al. [Kumbhojkar, N et al (1999)]. For the sample with 70mM concentration of the capping agent the shift in the absorption edge was not remarkable.

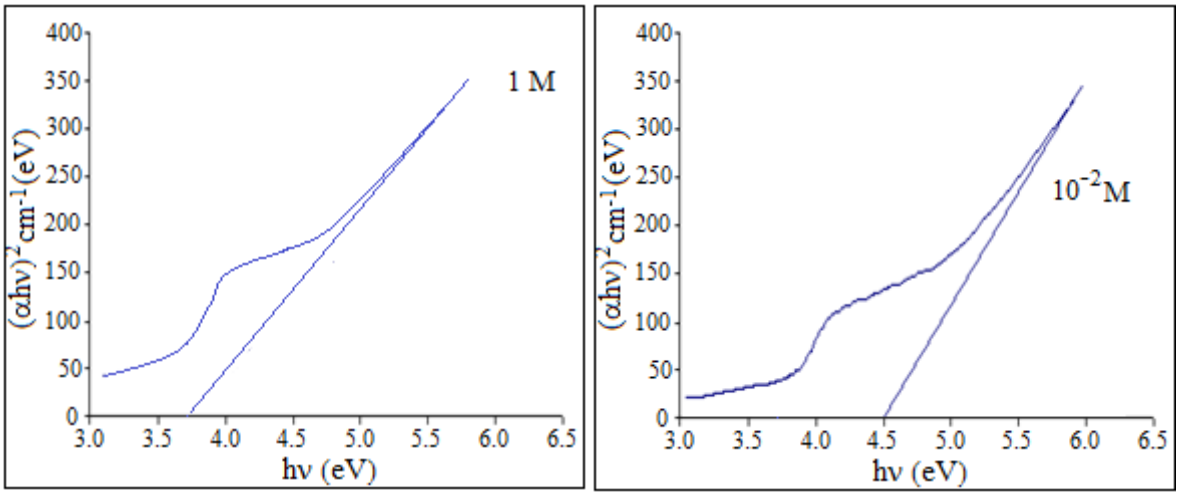

Fig. 5 Tau's plot of ZnS:Mn nanoparticles with different molar concentration

From the figure 5, it is very clear that the band gap for the sample with lower molar concentration is more than the band gap of the sample with higher molar concentration of the reactants. The band gap for higher concentration sample was calculated to be $\approx 3.75 \pm 0.05$eV and the band gap for the sample with lower concentration was $\approx 4.6 \pm 0.05$ες. This indicates that the particle size of the sample with lower concentration is less than that of the sample with the higher concentration. Even some of the samples were formed as colloidal solutions and could not be precipitated.

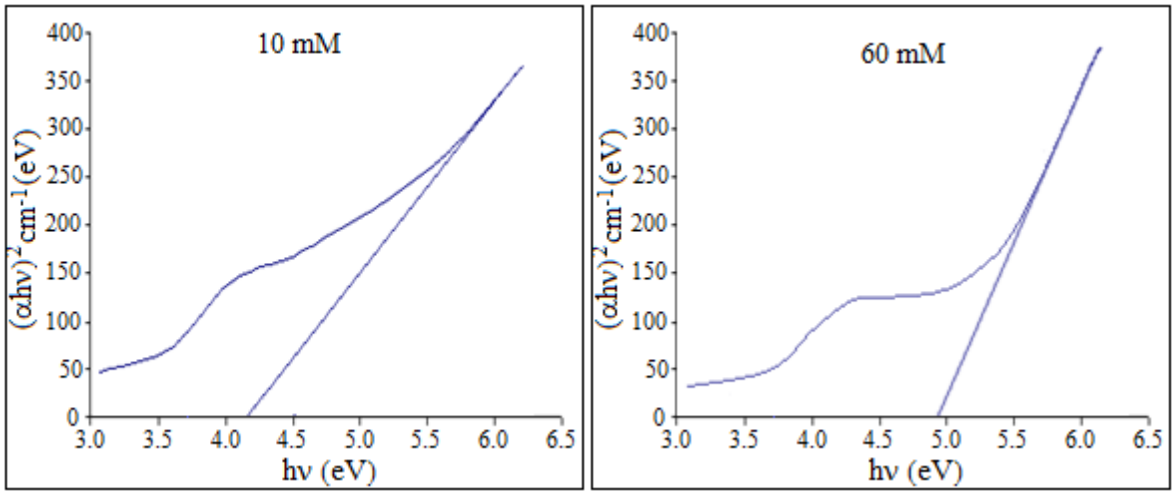

Fig. 6 Tau's plot of ZnS:Mn nanoparticles with different concentration of ME

Figure 6 shows the tau's plot of ZnS:Mn nanoparticles with different concentration of mercaptoethanol. Table 1 shows the band gap of ZnS:Mn nanoparticles with different concentration of ME. There is a shift of 2.34eV in the band gap as compared to the bulk ZnS (3.66eV). This is an indication that the capping agent played an important role in controlling the particle size.

Table 1 Band gap of ZnS:Mn nanoparticles

Concentration of ME	Band Gap
10mM	**4.2 □□0.05 eV**
20mM	**4.35 □□0.05 eV**
40mM	**4.8 □□0.05 eV**
60mM	**5 □□□0.05 eV**

The UV-visible absorption measured as a function of wavelength reflects the strength of the electronic transition between the valence bands (VB) and conduction bands (CB). The transition from the valence to the conduction band is the solid state analog to the HOMO-LUMO electronic transition in molecules. In the case of direct band gap transitions, typically a strong excitonic band with a well-defined peak is observed at the low energy side of the spectrum. The excitonic state is located slightly below the bottom of the conduction band. The energy difference between the bottom of the CB and the excitonic state is the electron-hole binding energy, which is typically a few to a few hundred meV. Thus, the peak position of the excitonic absorption band provides an estimate of the band gap of the nanoparticle. The band gap energy increases with decreasing particle size, resulting in a blue-shift of the

absorption spectrum as well as the excitonic peak. In contrast, indirect band gap transitions lack an excitonic peak and the spectrum usually features a gradually and smoothly increasing absorption with decreasing wavelength. Quantum confinement in indirect band gap materials is less easily observable due to the lack of sharp or well-defined spectral peaks or bands.

When the sizes of the nanoparticles become comparable to the Bohr excitonic radius (a_B), a quantum confinement effect is expected from these particles. The quantum confinement effect may be qualitatively understood using the particle-in-a-box model from quantum mechanics. In other words, a smaller box yields larger energy gaps between electronic states than does a larger box. The Bohr radius is given by [Bhattacharjee B. (2002)]

$$a_B = \frac{4\pi\varepsilon_0\varepsilon_r\hbar^2}{e^2}\left[\frac{1}{m_e^*} + \frac{1}{m_h^*}\right] \quad (1)$$

where **ε** is the dielectric constant, and m_e^* and m_h^* are the effective masses of electrons and holes, respectively. For spherical particles, the radius of the particles can be calculated by theoretical models.

There are two different theoretical models that are used to understand the variation of band gap with particle size (1) effective mass approximation (EMA) and (2) hyperbolic band model. The effective mass approximation (EMA) model and hyperbolic band model predicting the variation of excitation energy with particle size are used to estimate the crystalline size [L.E. Brus, J (1984), Kayanuma Y. (1998), Rosseti, R. et al (1984)]. We have used effective mass approximation model to calculate the particle size.

According to the effective mass approximation model the lowest excited state of the crystallite is assumed to be the ground state of an electron hole pair. The ground state energy of exciton or the increase in effective band gap as a function of crystalline size is estimated as

$$\Delta E = \frac{\hbar^2\pi^2}{2r^2}\left[\frac{1}{m_e^*} + \frac{1}{m_h^*}\right] - \frac{1.786\ e^2}{\varepsilon r} - \frac{0.124\ e^4}{h^2\varepsilon^2}\left[\frac{1}{m_e^*} + \frac{1}{m_h^*}\right]^{-1} \quad (2)$$

where ΔE is the blue-shift of the band gap, m^*_e is effective mass of electron, m^*_h is the effective mass of the hole, r is the radius of the particles and ε is the dielectric constant. The first term on the right hand side shows that the effective band gap is inversely proportional to r^2 and increases as size decreases. On the other hand, the second term shows that the band gap energy decreases with decreasing r due to increased Columbic interaction force and the last term corresponds to the correlation between the two particles. However, since the first term becomes dominant with small r, the effective band gap is expected to increase with decreasing r, especially when r is small. The effect of solvent or embedding environment is neglected in this form of the equation, but the effect of solution is typically small compared to quantum confinement. The second and third terms are much smaller than the first term therefore they can be neglected. Thus equation may be expressed as

$$\Delta E = \frac{\hbar^2\pi^2}{2r^2}\left[\frac{1}{m_e^*} + \frac{1}{m_h^*}\right] \quad (3)$$

The value of effective mass of electrons and holes for ZnS are $0.41m_e$ and $0.61m_e$ [Lippens, P.E. et al (1991)]**.** The particle size calculated from this model is given in the Table 2. It is seen that particle size estimated from absorption edge is of the same order as that obtained from TEM images.

Table 2 Particle Size of the samples

Samples of ZnS:Mn	Radius of particle in nm (r) EMA
1M molar concentration	4.38 nm
10^{-2} M molar concentration	1.28 nm
10 mM concentration of ME	1.67 nm
20 mM concentration of ME	1.50 nm
40 mM concentration of ME	1.16 nm
60 mM concentration of ME	1.07nm

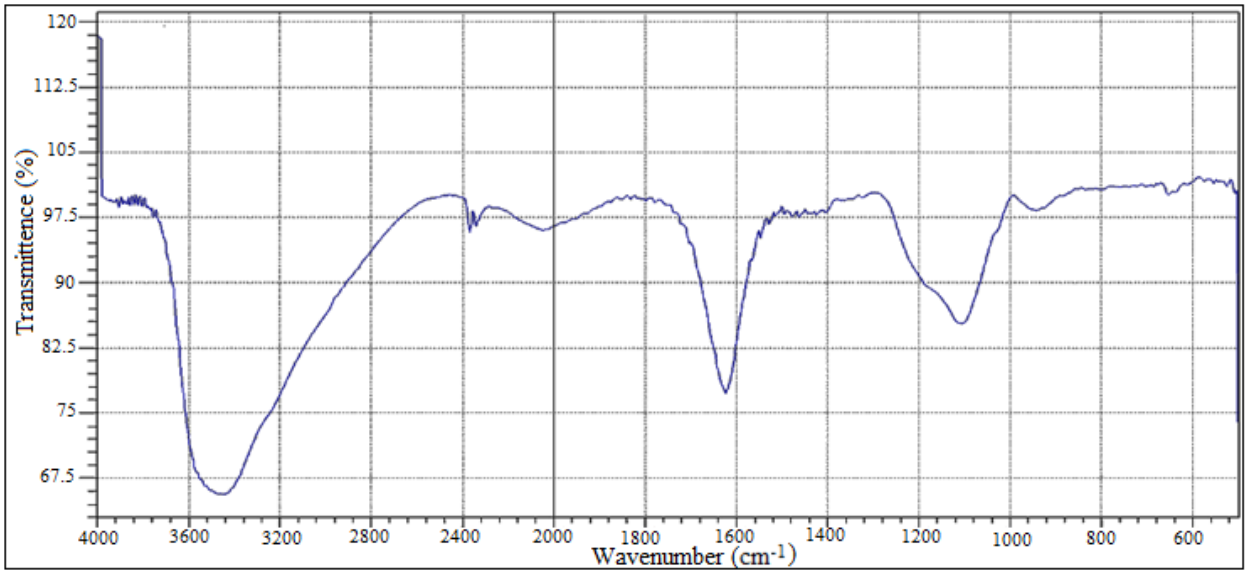

Fig. 7 FTIR spectra of ZnS:Mn nanocrystals

Figure 7 shows the FTIR spectra of ZnS:Mn nanocrystals at room temperature. The spectra show characteristic peaks at 1058, 1618, 2011, 2951, 3450 cm^{-1} and some other associated peaks. The peaks at 651 $cm^{-1}$is assigned to the ZnS band (i.e., corresponding to sulphides).Bands around 900-1500 cm^{-1} are due to the oxygen stretching and bending frequency. The peak at 2951 is assigned to the characteristic vibrations of the methylene groups in ME. The stretching vibration bands of the C–O groups on ME located at 1000–1300 cm^{-1} also bands around 1200 and 1100 cm^{-1} are due to the characteristic frequency of inorganic ions. These modes indicate the presence of resonance interaction between vibrational modes of sulphide ions in the crystal [Kurian S. et al (2004)]. The FTIR spectra showed peak at 1618 cm^{-1}, representing the nitrogen–oxygen interaction. The absorption peak of the S–H vibration at 2550–2565 cm^{-1} is not observed in the IR spectrum, indicating that the mercapto groups of the ME molecules were bound to the ZnS nanoparticle surface. Bands around 3000-3600 cm^{-1} are due to the hydrogen stretching frequency (O-H stretching). The band at 3450 cm^{-1} corresponds to characteristic vibration band of hydroxyl groups of ME molecules. The spectrum of the samples yields the bands, which are in good agreement with the reported values [Warad H C et al (2005), Rema Devi et al (2007)].

International Science Journal
(Peer-Reviewed)
ISSN: 2348 – 604X (p); 2348 – 6058 (e)

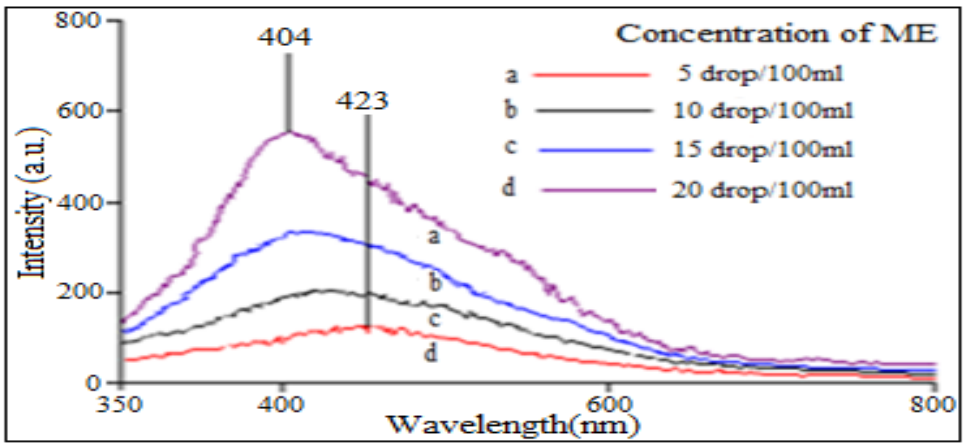

Fig.8 PL spectra of ZnS nanocrystals with different concentration of ME

Luminescence studies provide information regarding defect states. In nanocrystals, the defect states may shift or the density may increase which is revealed by PL studies. Fig.8 shows the PL spectra of ZnS samples (without Mn) in the range 350 nm-600 nm prepared with various concentration of capping agent (10mM – 60mM).The samples were excited at 289nm. Only one emission peak was obtained showing shifts towards shorter wavelength with the increase in the concentration of the capping agent. Stoke-shifted PL peak was obtained at 423 nm, 417 nm, 410 nm and 404 nm for 10mM, 20mM, 40mM and 60mM concentration of ME, respectively. It is visible that the PL emission becomes more intensive and shifts towards smaller wavelength as the size of the particles is decreased.

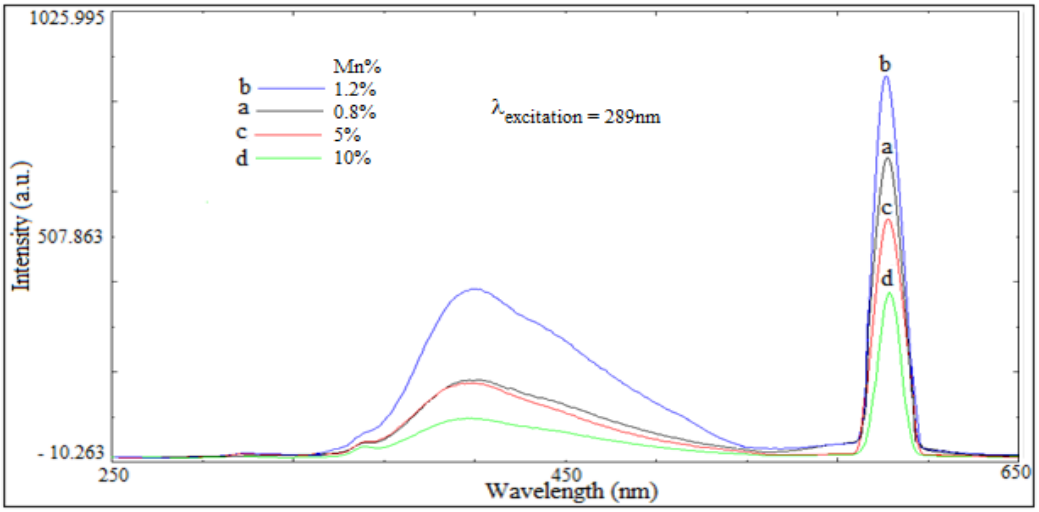

Fig.9 Photoluminescence of ZnS:Mn nanocrystals with different concentration of Mn

The figure 9 shows the PL spectra of ZnS : Mn nanoparticles with different Mn concentration. The concentration of capping agent (60 mM) was kept constant for all the samples. The concentration of Mn was changed from 0.8% to 10%. From the PL spectra, two peaks were found for each sample. The position of first peak was found at 408 nm

and the second peak was found at 583nm. The PL intensity changes for the samples with different concentration of Mn. Initially the PL intensity increases with increase in the Mn concentration. For 1.2 Mn% it is maximum and then it decreases with increasing Mn concentration. Due to the small particle size 1.8 ± 0.4 nm, surface defects such as donors and acceptors are easily formed on the ZnS nanocrystal surface. When an electron is prompted to the excited state, there are two main paths for the electron to relax to the ground state. One is the relaxation process through surface defects, such as donors and acceptors. This relaxation will usually give rise to a non-radiative recombination and/or light emission at other wavelengths. The other emission is due to an intraconfigurational $^3d_5$ transition on the Mn^{2+} ion located within the band gap of ZnS nanocrystals. This $^4T_1$ to $^6A_1$ energy transition gives rise to an orange photoluminescence. The decrease in PL intensity at with increasing Mn concentrations is due to concentration quenching effect [K.H. Yoon, J.K. Ahn and J.Y. Cho (2001)].

The luminescence mechanism can be understood by the energy level concept. The energy states within the band gap in the nanocrystals are produced due to surface states or Zn^{2+} or S^{2-} ions. The electrons are excited by the higher energy photons from the valance band (VB) or Zn^{2+} levels to the conduction band (CB). The excited electrons decay non-radiatively to surface-states and then decay radiatively to valance band and emit a photon of lower energy. When the particle size decreases, the valance band edge shifts downwards. Therefore, the emitted photon has comparatively higher energy giving photoluminescence peak at shorter wavelength. In ZnS nanoparticles, a large fraction of total number of atoms resides on the surface. The SH group of mercaptoethenol dissociates and organic group gets attached to Zn ions. Thus, the organic legends are instrumental in removing Zn dangling orbitals from the gap. The sp^3 hybridized orbital of surface S atoms dangle out of the crystal surface. More unsaturated S dangling bonds will be present on the surface. Hence, the legend terminated surfaces often show deep hole traps. These observations indicate that the PL peak obtained at shorter wavelength with reducing the particle size is due to hole traps, originating from unsaturated sp^3 orbital of surface S atoms.

4. CONCLUSIONS

The nanocrystals of Mn doped zinc sulphide have been successfully synthesized by a simple precipitation reaction using aqueous medium, in which mercaptoethanol was used as the capping agent. The XRD pattern indicated the growth of the nanoparticles. SEM images show the agglomeration of nanocrystals and therefore larger size was observed whereas XRD give the extent to which regular arrangement of atoms exists and hence gives the average crystal size. XRD analysis shows the sample prepared is in a cubical phase. TEM images indicated the growth of the nanoparticles, the particle size was found to be in the range 1nm -4nm. The particle size of nanocrystals was calculated both theoretically and experimentally and was found to be nearly in the same range. The measurement of optical absorption spectra shows blue-shift for the samples with different concentration of ME. The solid-state theory based on the delocalized electron and hole within the confined volume can explain the blue-shifted optical absorption spectra. Prominent IR peaks are analyzed and assigned. The FTIR spectra inferred that the stabilizing agent passivated the surface of the particles. The blue-shift in the peak position of photoluminescence spectra was also observed for the samples with decreasing particle size. The maximum PL intensity was recorded for the sample with 1.2 % of Mn.

REFERENCES

Barton J.C., Ranby P.W. (1997). *J. Phys.* E, 10: 437-438.
Bhargava R.N., Gallaghar D., Hong X., Nurmikko A. (1994). *Phys. Rev. Lett.* 72: 416-9.
Bhattacharjee B., D. Ganguli, K. Iakoubovskii, A. Stesmans and S. Chaudhuri. (2002). ***Bull****. Mater. Sci.* 25 : 179.
Bhattacharjee B., Ganguli D., Chaudhuri S., Pal A.K. (2003). *Mater. Chem. Phys*. 78: 372-379.
Bol A.A., and Meijerink A., J. Phys. Chem B., 105, 10203-9, (2001).
Borse P.H., Deshmukh N., Shinde R.F., Date S.K., Kulkarni S.K. (1999). *J. Mat. Sci.* 34: 6087-6093.
Brus L.E. (1984). J. Chem. Phys. 80 : 4403.

Cao G. (2004). Nanostructures and Nanomaterials: Synthesis, Properties and Applications; Imperial College Press, London.
Chen W., Wang Z., Lin Z., Lin L. (1997). *J. Appl. Phys.* 82: 3111-15.
Chen J., Li Y., Wong Y., Wong J., Yun J., Cao D. (2004). Mater. Res. Bull. 39: 185-194.
Dalacu N., Kitai A.H. (1991). *Appl. Phys. Lett.* 58: 613-15.
Ghrayeb J., Jackson T.W., Daniels R., Hopper D.G. (1997). *Proc. SPIE.* 3057: 237-240.
Guinier A. (1963). X-ray Diffraction, Freeman, San Francisco.
Karar N. Singh F., Mehta B.R. (2004). *J. Appl. Phys.* 95, 656-660.
Kayanuma Y. (1998). *Phys. Rev.* B., 38 : 9797.
Khosravi A.A., Kundu M., Shekhawat G.S., Gupta R.R., Sharma A.K., Vyas P.D., Kulkarni S.K. (1995). Appl. Phys. Lett. 67: 2506-2508.
Kumbhojkar N., Nikesh V.V., Kshirsagar A. and Mahamuni S. (1999). *J. Appl. Phys*. 88(11) : 6260.
Kurian Sibi, Sebastian Shajo, Mathew Jose and George K. C. (2004). *Indian J. Pure Appl. Phys.* 42: 926-933.
Lippens, P.E., Lannoo, M. (1991). *Semicon. Sci. Tech.* 6 : 157.
Lu H.-Y., Chu S.-Y., Tan S.-S. (2004). *J. Cryst. Growth.* 269: 385-391.
Mandal S.K., Chaudhuri S., Pal A.K. (1999). *Thin Solid Films*. 30: 209-13.
Nanda J., Sarma D.D. (2001). *J. Appl. Phys.* 90 : 2504-2510.
Nanda J., Sapra S., Sarma D.D.Chandrasekharan N. and Hodes G. (2000). *Chem. Mater.* 12: 1018-22.
Ni Y., Yin G., Hong J. Xu, Z. (2004). *Mater. Res. Bull.* 39 : 1967-1972.
Okuda H., Dakada J., Iwasaki Y., Hashimoto N., Nagao C. (1990). IEEE Trans. Consumer Electron., 36: 436-439.
Peng W.Q., Qu S.C., Cong G.W., Wang Z.G. (2005). *J. Crystal Growth.* 279: 456.
Que W., Zhou Y., Lam Y.L., Chan Y.C., Kam C.H., Liu B. et. Al. (1998). *Appl. Phys. Lett.* 73: 2727-2729.
Rema Devi B S, Raveendran R and Vaidyan A V. (2007). Pramana. 68(4): 679-687.
Rosseti R., Ellison, J.L., Gibson, J.M., Brus L.E. (1984). *J. Chem. Phys.* 80(9): 4464.
Scholtz S.M., Vacassy R., Dutta J., Hoffmann H. (1998). *J. Appl. Phys.* 83: 7860-7866.
Strukov D.B., Snider G.S., Stewart D.R. (2008). Williams R.S., *Nature.* 453: 80-83.
Tan M., Cai W., Zhang L. (1997). *Appl. Phys. Lett.* 71: 3697.
Warad H C, Ghosh S C, Hemtanon B, Thanachayanont C and Dutta J. (2005). Science Technol. Adv. Mater., 6, 296-301.
Xu J.F., Ji W., Lin J.Y., Tang S.H., Du Y.W. (1998). *Appl. Phys*. A 66: 639-641.
Yoon K.H. Yoon, Ahn J.K. and Cho J.Y. (2001). *J. Mater. Sci.* 36: 1376.
Zhao Y., Hong J.M., Zhu J.J. (2004). *Cryst. Growth.* 270: 438-445.

